NIH Public Access
Author Manuscript
J Biol Inorg Chem. Author manuscript; available in PMC 2010 December 27.

Published in final edited form as:
J Biol Inorg Chem. 2010 September ; 15(7): 1051–1062. doi:10.1007/s00775-010-0664-8.

THE EFFECT OF PHOSPHATE ACCUMULATION ON METAL ION HOMEOSTASIS IN *SACCHAROMYCES CEREVISIAE*

Leah Rosenfeld, **Amit R. Reddi**, **Edison Leung**, **Kimberly Aranda**, **Laran T. Jensen***, and **Valeria C. Culotta**✉
Department of Environmental Health Sciences, Johns Hopkins University Bloomberg School of Public Health, Baltimore, MD 21205, USA

Abstract

Much of what is currently understood about the cell biology of metals involves their interactions with proteins. By comparison, little is known about metal interactions with intracellular inorganic compounds such as phosphate. Here we examined the role of phosphate in metal metabolism *in vivo* by genetically perturbing the phosphate content of *Saccharomyces cerevisiae* cells. Yeast *pho80* mutants cannot sense phosphate and have lost control of phosphate uptake, storage and metabolism. We report here that *pho80* mutants specifically elevate cytosolic and non-vacuolar phosphate and this in turn causes a wide range of metal homeostasis defects. Intracellular levels of the hard metal cations sodium and calcium increase dramatically, and cells become susceptible to toxicity from the transition metals manganese, cobalt, zinc and copper. Disruptions in phosphate control also elicit an iron starvation response, as *pho80* mutants were seen to up-regulate iron transport genes. The iron responsive transcription factor Aft1p appears activated in cells with high phosphate in spite of normal intracellular iron levels. The high phosphate of *pho80* mutants can be lowered by mutating Pho4p, the transcription factor for phosphate uptake and storage genes. Such lowering of phosphate by *pho4* mutations reversed the high calcium and sodium of *pho80* mutants and prevented the iron starvation response. However, *pho4* mutations only partially reversed toxicity from heavy metals, representing a novel outcome of phosphate dysregulation. Overall these studies underscore the importance of maintaining a charge balance in the cell; a disruption in phosphate metabolism can dramatically impact on metal homeostasis.

Keywords

yeast; manganese; Aft1; Pho80; polyphosphate

Introduction

In the cell, inorganic elements that range from the alkali and the alkaline earth metals (e.g., sodium, potassium, magnesium, calcium) to transition metals (e.g., manganese, cobalt, iron, zinc copper) serve important biological functions in signaling and structure, and act in the catalytic center of numerous enzymes. Although much of what is currently known about metal homeostasis involves their interaction with proteins and other organic macromolecules, metal cations can also bind small negatively charged inorganic compounds, such as phosphate. Phosphate readily forms complexes *in vitro* with a wide range of metals [1]. In some instances, such interactions can alter the reactivity of the cation,

✉To whom correspondence should be addressed: Johns Hopkins University Bloomberg School of Public Health, 615 N. Wolfe Street, room E7626, Baltimore, MD, fax (410)955-0116, vculotta@jhsph.edu.
*Current address: Department of Biochemistry Faculty of Science, Mahidol University, 272 Rama VI Road, Bangkok 10400, Thailand

NIH-PA Author Manuscript
NIH-PA Author Manuscript
NIH-PA Author Manuscript

NIH-PA Author Manuscript

NIH-PA Author Manuscript

NIH-PA Author Manuscript

particularly redox active transition metals [2,3]. As phosphate is relatively abundant in cells, and can potentially bind a variety of metal cations, metal-phosphate interactions should be taken into account when exploring the mechanisms regulating metal homeostasis in the cell.

In organisms ranging from bacteria to mammals, phosphate is stored in the form of orthophosphate (P_i), pyrophosphate, and long polymers of polyphosphate which have been found in a range of organelles [4,5]. With the abundance and widespread distribution of phosphate in cells, one might predict a link between phosphate and cation homeostasis. Indeed, bacteria and plants can guard against toxicity of non-essential heavy metals such as mercury, cadmium and lead through sequestration of these ions by intracellular polyphosphate [6–8]. Extracellular phosphate in the growth medium can also affect metal homeostasis at the level of metal uptake from the environment. For example, in the bakers yeast *S. cerevisiae*, phosphate and cation uptake are linked through two phosphate transporters, Pho89p and Pho84p. Pho89p is a Na^+-coupled phosphate co-transporter that works primarily at alkaline pH [9] whereas Pho84p is metal-phosphate transporter that can contribute to accumulation of toxic concentrations of manganese and cobalt when these metals are present in excess in the growth medium [10,11].

Bakers' yeast represents a useful model system with which to study the interaction between phosphate and metals. Phosphate uptake and storage are controlled by the cyclin dependent kinase (CDK)-cyclin pair, Pho85p-Pho80p. When phosphate is abundant, Pho85p-Pho80p is an active kinase and negatively regulates phosphate uptake and storage. When phosphate is scarce, IP_7 (myo-D-inositol heptakisphosphate) accumulates and leads to inactivation of Pho85p-Pho80p; phosphate uptake and storage genes are then induced [12,13]. Induction of these genes is accomplished by the Pho4p transcription factor. During phosphate-replete conditions, Pho85p-Pho80p phosphorylates Pho4p, which causes the transcription factor to be excluded from the nucleus. When conditions are phosphate-limited, Pho85p-Pho80p fails to phosphorylate Pho4p and the transcription factor is free to activate the promoters of phosphate uptake and storage genes including the aforementioned *PHO89* and *PHO84* [14–16].

In this study we manipulated the Pho80p-Pho85p system of bakers' yeast to examine the effect of phosphate on metal ion homeostasis. We report here that a *pho80*Δ mutation specifically leads to a rise in cytosolic or extra-vacuolar phosphate and this elevated phosphate correlates with a wide spread effect on metal cation accumulation, bioavailability and toxicity. These effects range from a drastic elevation in accumulation of sodium and calcium, to increased sensitivity towards toxicity from manganese, cobalt, zinc and copper to the induction of an iron-starvation response. The underlying mechanism of these effects including relevant signaling pathways and gene expression changes are probed herein.

Materials and Methods

Strains, and Growth Conditions

All the strains in this study are isogenic to BY4741 (*Mat**a**, leu2*Δ*0, met15*Δ*0, ura3*Δ*0, his3*Δ*1*). Commercially available deletions (Open Biosystems) were verified using DNA sequencing and include LR801 (*pho80*Δ *::KanMX4)*, LR802 (*pmr1*Δ*::KanMX4)*, LR803 (*pho85*Δ*::KanMX4)*, and 1090 (*aft2*Δ*::KanMX4)*. Construction of LR181 (*pho4*Δ*::LEU2*) and LR191 (*pho80*Δ*::KanMX4 pho4*Δ*::LEU2*) was carried out using the previously published *pho4::LEU2* plasmid (kind gift of Joaquin Arino, Universitat Autonoma Barcelona) [17]. *PHO84* was disrupted in BY4741 and in LR801 to create LR122 (*pho84*Δ*::LEU2*) and LR154 (*pho80*Δ*::KanMX4 pho84*Δ*::HIS3*) using the previously published pLJ246 [11] and pLJ089 [18] *pho84* deletion plasmids. Genetic deletion of *aft1*Δ in LJ194 (*aft1*Δ*::LEU2)* and LJ416 (*aft1*Δ*::LEU2 pho80*Δ*::KanMX4)* was carried out using

NIH-PA Author Manuscript

NIH-PA Author Manuscript

NIH-PA Author Manuscript

pLJ176 as previously described [19]. LR237 (*pho80Δ::LEU2*) and AR086 (*pho80Δ::LEU2 aft2Δ::KanMX4*) were constructed using the pLR001 deletion plasmid in strains BY4741 and 1090, respectively.

Cells were maintained by growth at 30°C in either enriched YPD (1% bacto-yeast extract, 2% bacto-peptone, 2% dextrose), SC (synthetic complete) media, or low phosphate SC media made as described [18]. Growth media had 2% agarose added for solid media. For metal toxicity tests, 10^5, 10^4, 5×10^2 and 30 cells were spotted onto solid YPD medium supplemented with defined metal concentrations and allowed to grow at 30°C for 48 hours.

Vacuolar and cytosolic fractions were prepared as described by Yang *et al*. [20], with the following modifications. Cells were grown overnight in YPD from a starting OD_{600nm}=0.05. The next day, the cells were diluted into 1 L of YPD media to an OD_{600nm} =0.2 and grown to OD_{600nm} =2.0. Prior to spheroplast preparation as described previously, [20] cells were washed with ice cold water. Vacuolar and cytosolic fractions were collected using a Ficoll density gradient [20]. The purity of the vacuolar and cytosolic fractions was monitored by Western blot analysis using antibodies directed against CPY (carboxypeptidase Y) and PGK1 (phosphoglycerate kinase 1), which are markers for the vacuole and cytosol, respectively.

The *PHO80* disruption plasmid pLR001 was generated by PCR amplifying the upstream (−850 to −98) and downstream sequences (+180 to +627) introducing BamHI and NotI or SalI and BamHI sites, respectively. The *PHO80* PCR products were digested with the indicated enzymes and ligated in a trimolecular reaction into pRS305 (*LEU2*) digested with SalI and NotI, resulting in pLR001. Transformation of yeast strains with pLR001 digested with BamHI resulted in deletion of *PHO80* sequences from −98 to +180.

Plasmids

The LacZ reporter plasmids used in this study include the previously published pLJ051 (spanning −900 to +1 of the *FET4* promoter respectively) [21], and pFC-W (described herein as *AFT-CYC*) with the Aft1p recognition sequence of the *FET3* promoter fused to the core *CYC1* promoter (gift from D. Winge, U. Utah) [22,23]. The following LacZ fusion constructs were all based on pLJΔ178 and constructed as previously described [21]: pLJ098, −813 to +3 of *ACT1*; pLJ439, −777 to +3 of *ARN2*; pLJ440, −733 to +1 of *FET3* and pLJ441 −783 to +1 of *FRE4*.

Biochemical Assays

ICP-MS (inductively coupled plasma mass spectroscopy) analysis was carried out using an Agilent 7500ce ICP–MS according to manufacturer specifications, and values were converted to nmol metal/10^9 cells or μMolar using an average size of 7×10^{-14} L/cell [24]. For analysis, triplicate overnight cultures were grown in YPD medium, washed twice with MilliQ water and 20 OD_{600} units of cells were concentrated and digested overnight in 1 mL 20% nitric acid at 95°C. Cell debris was removed by centrifugation and samples diluted to 2% nitric acid for analysis. In order to determine the manganese and iron content of the cytosolic and vacuolar fractions, atomic absorption spectroscopy (AAS) analysis for measurements of whole cell manganese was carried out on a PerkinElmer Life Sciences AAnalyst 600 graphite furnace atomic absorption spectrometer according to the manufacturer's specifications, as described [11]. A concentration of .1 mg/mL of protein from the vacuolar and cytosolic fractions was sufficient for quantitating iron and manganese using this method. Phosphate content of the vacuolar and cytosolic fractions as well as whole cell lysates was determined using the colorimetric molybdate assay as described previously [18]. Total phosphate was measured from boiling 3–30 μg of protein from

NIH-PA Author Manuscript
NIH-PA Author Manuscript
NIH-PA Author Manuscript

vacuolar, cytosolic and whole cell lysate fractions for 10 min in 1 N H_2SO_4. Orthophosphate was measured from unboiled samples. Polyphosphate (PolyP) is taken as the difference between the boiled and unboiled samples [25]. Polyphosphate was also directly detected using polyacrylamide gel electrophoresis and toluidine blue staining as described [18].

RNA and promoter activity measurements

For microarray analysis, duplicate cultures of WT and *pho80* mutants were grown in YPD +75 μM $MnCl_2$ to an $O.D._{600}$ approximately equal to 1.0. Manganese was added to cultures to detect any mRNA changes in *pho80*Δ cells under metal toxicity conditions; however, the changes in phosphate metabolism and iron transport genes reported here were found to be independent of such manganese treatment. Cells were harvested and RNA extracted using the hot phenol method [25]. RNA was converted to cDNA and cRNA according to manufacturers specifications (Affymetrix) and was subject to analysis using the Affymetrix GeneChip® Yeast Genome 2.0 Array. In this study, four pairwise comparisons were used (*pho80*Δ, *n* = 2 *versus* WT, *n* = 2). Fold change (FC) was calculated as recommended by the manufacturer; for gene with a Signal Log Ratio >0, $FC=2^{\text{Signal log ratio}}$; for genes with a Signal Log Ratio <0, $FC=-2^{-\text{Signal log ratio}}$. The subset of genes involved in phosphate metabolism and iron transport are shown in Table 2.

RNA for Real Time PCR was isolated identically as that described above for microarray analysis from cultures grown under the same conditions. Genomic DNA contamination was removed using Applied Biosystems TURBO DNase according to the manufacturer's specifications. Total RNA (2 μg) was used for cDNA synthesis using the Applied Biosystems High Capacity cDNA Reverse Transcription Kit according to manufacturer's directions. Quantitative PCR reactions were completed using Taqman PCR master mix and FAM fluorophore (6-carboxyfluorescein) labeled probes. Primers and probes were designed by Applied Biosystems using the Filebuilder 3.1 program. Primers used were shown to yield an equal change in cycle threshold number (C_T) over four orders of magnitude change in RNA levels and were validated by the absence of signal from the corresponding yeast deletion mutant. *ACT1* mRNA was used for normalization. Fold change was calculated as follows: The normalized threshold cycle was calculated as $\Delta C_T = C_T(\text{target gene}) - C_T(\textit{ACT1})$. The fold change (FC) was then calculated by $FC = 2^{-(\Delta C_T \text{ (yeast strain of interest)} - C_T(\text{wild type}))}$.

LacZ reporter assays were carried out according to published protocols [21].

Results

Loss of yeast PHO80 affects metal homeostasis

To examine the effect of phosphate on ion homeostasis, we used a yeast mutant with a deletion in the *pho80* cyclin gene. Yeast lacking *pho80* are disrupted for phosphate sensing and are known to hyper-accumulate phosphorus and phosphate (3–10 fold) especially in enriched medium [15,18]. By comparison, phosphorus levels rise by no more than 50% when *pho80* mutants are grown in a synthetic minimal medium (Supplementary Table 1) presumably due to the low activity of the Pho84p phosphate transporter in this medium [18]. Therefore, the *pho80* mutant grown in enriched medium provided an excellent model system in which to test the impact of phosphate on metal homeostasis.

As seen in Fig. 1, the elevated phosphorous of *pho80* mutants correlated with various increases in cellular metals. The most dramatic effect was on calcium and sodium, where intracellular levels rose by nearly 10 and 100 fold respectively in the *pho80* mutant. When grown in enriched medium, WT cells concentrate calcium but accumulate lower levels of sodium than the external medium (Table 1), and these trends are consistent with previous

NIH-PA Author Manuscript

NIH-PA Author Manuscript

NIH-PA Author Manuscript

studies [26]. Yet with the *pho80* mutant, both cations are elevated with respect to the growth medium (Table 1). Aside from the dramatic effects on sodium and calcium, *pho80* mutations were also associated with a 1.5 – 2 fold increase in potassium and magnesium, as well as with the transition metals manganese, cobalt, iron and zinc (Figure 1 and Table 1).

We addressed whether the increased metal accumulation of *pho80* mutants correlated with increased sensitivity towards these elements. As seen in Fig. 2A, *pho80* mutants exhibited increased sensitivity towards high calcium and sodium in the enriched growth medium consistent with very high intracellular levels of these cations (Fig. 1). Sensitivity towards the heavy metals manganese, cobalt, zinc and copper was also increased by *pho80* mutations (Fig. 2A) in spite of the small effects of *pho80* on accumulation of these metals under normal growth conditions (i.e., no metal surplus) (Fig. 1). At least in the case of manganese, this reflected increased metal accumulation during metal surplus conditions. As seen in Fig. 2B, *pho80* mutants exhibit a dramatic elevation in intracellular manganese levels compared to wild type cells when cells are treated with increasing doses of extracellular manganese.

Mutations in pho80 stimulate an iron-starvation response

In addition to the aforementioned effects on metal toxicity, *pho80* mutants exhibit an apparent iron starvation state. This impact on iron homeostasis was initially noted during a global gene array analysis of *pho80* mutants. The cells not only exhibit the anticipated induction of phosphate regulated genes (e.g., *PHO5, PHO89, PHM6* and *SPL2* [15]), but show an increased expression of genes typically induced by iron starvation. These genes included *ARN2, FIT2, FIT3,* and *FRE4* involved in iron siderophore transport and retention [27,28] (Table 2). Results were confirmed by real time PCR measurements of mRNA from *pho80* versus WT strains grown in enriched medium (Table 3). We also analyzed the iron-regulated genes through promoter fusions experiments in which the upstream non-coding region for these genes were fused to bacterial *lacZ.* As seen in Fig. 3A, the promoter activity for *ARN2* and *FRE4* was increased 5–10 fold in *pho80* mutants while an *ACT1* (encoding actin) promoter fusion control was unaffected.

ARN2, FIT2, FIT3 and *FRE4* are all targets of the Aft1p transcription factor that responds to iron starvation [29–31]. When iron is abundant, Aft1p localizes to the cytosol, but when cells are starved of iron, Aft1p accumulates in the nucleus where it activates genes involved in iron uptake and storage. The aforementioned *ANR2, FIT2, FIT3* and *FRE4* as just 4 out of 17 known iron transport and storage genes that serve as targets of Aft1p [32]. Other targets include genes for high and low affinity elemental iron transport *FET3* and *FET4* [31,33]. Changes in their expression were not detected in our microarray analyses; however *FET3* and *FET4* are induced ≈2 fold by *pho80* mutations as evidenced by the *lacZ* reporter assay (Fig 3B). The *FET3* reporter in particular required a low (1 mM) phosphate medium to observe induction. Overall, the most striking effects of *pho80* mutations were on the siderophore transport genes. The weak induction of the high affinity iron transport gene *FET3* might explain why *pho80* mutants only mildly hyperaccumulate iron (Figure 1).

Aft1p binds to a consensus sequence PyPuCACCC [32] and we tested whether a minimal promoter containing only this regulatory sequence was responsive to *pho80* mutations. This synthetic minimal promoter denoted herein as *AFT-CYC* comprises the isolated Aft1p binding site for *FET3* fused to the core promoter sequence for a heterologous gene (*CYC1*) and the *lacZ* reporter. *AFT-CYC* was previously shown to be an excellent reporter for Aft1p activation by iron starvation [23,30]. As seen in Fig. 3C, *AFT-CYC* is induced ≈5 fold in *pho80* mutants and unlike the native *FET3* promoter does not require a special low phosphate iron medium to observe induction. Apparently the complex intact *FET3* promoter contains other elements that preclude strong induction in *pho80* mutants. In any case, the strong activation of *AFT-CYC* demonstrates that the isolated Aft1p binding site can respond

NIH-PA Author Manuscript

NIH-PA Author Manuscript

NIH-PA Author Manuscript

to *pho80* mutations. To more directly test the role of the Aft1p transcription factor, we deleted the *AFT1* gene in the *pho80* strain. As seen in Fig. 3C, induction of *AFT-CYC* by *pho80* mutations was completely reversed upon deleting *AFT1*. Although *AFT-CYC* expression levels were greatly reduced in the *pho80 aft1*Δ double mutant, these levels were still higher than that observed with the single *aft1*Δ mutant (Fig. 3C); hence, some residual induction by *pho80* mutations can occur in the absence of Aft1p.

Yeast expresses a paralog of Aft1p known as Aft2p that can activate a similar set of iron transport genes [32]. We tested whether Aft2p contributed to *pho80* induction of iron metabolism genes. As seen in Fig. 3C, an *aft2*Δ gene deletion had no effect on the basal or *pho80*-induced expression of *AFT-CYC*, consistent with the notion that Aft1p, and not Aft2p, is the predominant regulator of the iron starvation response in *S. cerevisiae* [32]. Yet in the absence of Aft1p, it is possible that Aft2p contributes to the residual *AFT-CYC* induction we observe in the *pho80 aft1*Δ strain (Fig. 3C). The triple *pho80*Δ *aft1*Δ *aft2*Δ strain needed to confirm this notion proved to not be viable, most likely due to a severe iron starvation defect (not shown).

In addition to accumulating high phosphate, *pho80* mutants are associated with high levels of sodium (Fig. 1 and Table 1). However, this elevated sodium does not appear responsible for the observed Aft1p activation as WT strains treated with exceeding high concentrations of sodium did not induce *AFT-CYC* (Supplementary Figure 1). To test whether elevated phosphate was responsible, intracellular phosphate levels were reduced by introducing a mutation in *PHO4* encoding the transcription factor for phosphate uptake and storage genes. As seen in Figures 1 and 5A, the high phosphorus and phosphate of *pho80* mutants was reversed in the *pho80*Δ *pho4*Δ double mutant. This reduction in phosphate correlated with a reversal in the *pho80* induction of the iron starvation response as seen in the *AFT-CYC* reporter assay (Fig. 3D). The strong correlation between high intracellular phosphate and the iron starvation response indicates that phosphate is limiting bioavailability of the metal.

As one possibility, phosphate might be sequestering iron in the vacuole. To address this, vacuolar and cytosol preparations were obtained from WT cells and *pho80* mutants and subjected to phosphate analysis and measurements of iron. Surprisingly, vacuolar phosphate, both ortho and polyphosphate, was not significantly altered in the *pho80* mutant compared to WT (Fig. 4B, left). All the elevated phosphate of *pho80* mutants arises from phosphate accumulation in the cytosol or extra-vacuolar compartment (Fig. 4B, right). Consistent with the lack of increased vacuolar phosphate, there was no increased partitioning of iron towards the vacuoles of *pho80* mutants and the same is true for manganese (Fig. 4C). Hence the apparent iron starvation response of *pho80* mutants is not due to vacuolar sequestration of the metal, but perhaps due to increased iron-phosphate interactions in the cytosol or other compartments of the cell.

The contribution of phosphate to pho80 effects on metal accumulation and metal toxicity

As described above, the *pho4* gene mutation provides an ideal tool to reverse elevated phosphate in *pho80* mutants. We therefore used *pho4* mutations to test the effects of reducing intracellular phosphate on metal ion levels (as in Fig. 1) and on metal toxicity (as in Fig. 2A). As seen in Figure 1, the lowering of phosphate by *pho4* mutations resulted in a complete reversal of the very high sodium and calcium of *pho80* mutants. By contrast, a similar lowering of phosphate did not completely reverse the *pho80* sensitivity towards heavy metal toxicity. The *pho80 pho4* double mutant was only slightly more resistant to the toxicity of 2 mM manganese than the *pho80* single mutant and the two strains were equally sensitive to the toxicity of 4 mM manganese (Fig. 5B). Similarly, the *pho4* mutation only partially rescued the toxicity of the *pho80* mutant to cobalt and copper. Overall, the *pho80 pho4* mutant was still more sensitive to metal toxicity compared to the single *pho4* mutant or

NIH-PA Author Manuscript

NIH-PA Author Manuscript

NIH-PA Author Manuscript

WT strain, even though total cellular phosphate was low. Unlike the aforementioned elevations in calcium and sodium and the induction of iron response genes, the metal toxicity of *pho80* mutants cannot be easily attributed to high phosphate.

The Pho4p transcription factor is known to regulate *PHO84*, encoding the metal-phosphate transporter [11,34]. By Real Time PCR, we noted that transcript levels of *PHO84* were increased roughly 6 fold in *pho80* mutants (Table 3). Since Pho84p is a major contributor of cellular phosphate in enriched medium [11], we tested the effects of deleting *PHO84* on phosphate and metal accumulation in *pho80* mutants. As seen in Figs. 1 and 5A, *pho84* mutations dramatically lowered phosphorus and phosphate levels of *pho80* mutants grown in enriched medium and likewise reversed the high sodium and calcium of *pho80* mutants (Figs 1 and 5A). The high manganese accumulation of the *pho80* mutant grown in enriched medium was also completely reversed by *pho84*Δ mutations (Fig. 6A). Although Pho84p is a major transporter of phosphate in enriched medium, its contributions to phosphate in synthetic medium are minimal [18] and as such, *pho84* mutations only partly reversed the *pho80*-induction of the iron starvation response as analyzed by *AFT-CYC* expression in synthetic medium (Fig 3D).

While Pho84p contributes to manganese accumulation in *pho80* mutants (Fig. 6A), it is not the primary cause of metal toxicity. As seen in Fig. 6B, the *pho80 pho84* mutant is still more sensitive to manganese than the single *pho84* mutant in spite of accumulating very low manganese (Fig. 6A). Likewise, the *pho80* mutation still increased sensitivity towards cobalt and copper in strains lacking the Pho84p metal-phosphate transporter (Fig. 6B). Together these studies indicate that in *pho80* mutants, that enhanced metal uptake by Pho84p only partially accounts for the metal toxicity observed. There remains a component to the metal toxicity that is independent of Pho84p as well as the Pho4p transcription factor.

Discussion

With the large number of cellular processes that rely on phosphate, the uptake and storage of phosphate must be tightly controlled. Based on the natural affinity of phosphate compounds with metals, one might predict a linkage between phosphate and metal metabolism. This prediction was directly tested in these studies using yeast *pho80* mutants that hyper-accumulate phosphate. We find that loss of phosphate control in *pho80* mutants has wide spread effects on homeostasis of biologically relevant metals when the cells are grow in rich medium. These effects range from dramatic (10–100 fold) rises in steady state levels of the hard metal cations calcium and sodium, to increases in toxicity from the transition metals manganese, cobalt, zinc and copper, to activation of an iron starvation response.

We observed that a subset of effects of *pho80* mutations on metal cations is due to up-regulation of Pho84p, the metal-phosphate transporter. Pho84p has previously been shown to transport phosphate complexes of manganese and cobalt [10] and our earlier genetic studies suggested a similar role for Pho84p in transport of zinc and copper as well [11]. However, a role for Pho84p in uptake of hard metal cations including magnesium, potassium, sodium and calcium has not been previously noted, and in fact magnesium has been shown to inhibit Pho84p transport activity [10,11]. Pho84p may not be transporting complexes of calcium and sodium, rather the elevation of these elements in *pho80* mutants could represent a secondary consequence of high phosphate. These cations may enter the cell as a counter ion to balance the negative charge imposed by increased phosphate, although this is not sufficient to increase total cell volume as monitored by microscopy (not shown). The sequestration of calcium and sodium by high intracellular phosphate could be sensed as a calcium and/or sodium starvation state, stimulating transport systems for these cations. This is analogous to what we observe for phosphate effects on iron. Despite

NIH-PA Author Manuscript

NIH-PA Author Manuscript

NIH-PA Author Manuscript

relatively normal levels of iron, *pho80* mutants appear starved for iron, and genes involved in iron uptake and storage are induced. We find that *pho80* mutants accumulate elevated levels of ortho- and polyphosphate in the cytosol, but not in the vacuole. It is therefore likely that phosphate binding to metal cations in the cytosol decreases the bioavailability of these ions, resulting in a cation starvation stress response.

Although many effects of *pho80* mutations can be ascribed to Pho4p induction of Pho84p metal-phosphate transport, there exists a *PHO4* and *PHO84*-independent component to the increased toxicity from manganese, cobalt and copper. In our search thus far for this Pho4/Pho84 independent pathway, we have excluded a number of candidates. For example, *pho80* mutations still confer toxicity in a Pho4/Pho84 independent manner when the genes that affect synthesis (*VTC4* [15]), degradation (*PPN1* [35]) and intracellular localization (*PHO91* [34,36]) of polyphosphate are deleted. We have likewise excluded another downstream transcription factor phosphorylated by Pho80p, Rim15p [37,38], various manganese and iron transporters (Fet4p [39], Smf1p and Smf2p [40]), as well as the aforementioned Aft1p and Aft2p iron regulators (data not shown). New as of yet unidentified target(s) of Pho80p must be involved and this is under current investigation.

Finally it is worth mentioning that previous studies in bacteria and plants have indicated that high phosphate can be protective against metal toxicity presumably by phosphate sequestration of the metals [6–8]. By contrast, our studies in *S. cerevisae* argue that phosphate can augment metal toxicity both by promoting metal uptake (via Pho84p) and by another effect on metal homeostasis that is independent of metal uptake. Cellular phosphate could influence metal toxicity through formation of metal-phosphate complexes that directly cause toxicity, as has been proposed for the potent Mn^{+3}-phosphate oxidant [41]. In any case, these studies underscore the importance of maintaining a balance of charge in the cell and that disruptions in an abundant anion such as phosphate can have a dramatic and widespread impact on homeostasis of biologically important metals.

Supplementary Material

Refer to Web version on PubMed Central for supplementary material.

Acknowledgments

We wish to thank D. Winge and J. Arino for plasmids. We thank J. Mihalic for help with ICP-MS analysis. This work was funded by the JHU NIEHS center and by NIH grant ES 08996. L.R. and A.R were supported by NIEHS training grant ES 07141 and A.R. by an NIH/NIGMS fellowship F32GM093550. ICP-MS analysis was supported in part by the Maryland Cigarette Restitution Fund Program at Johns Hopkins and the NIEHS Center P30 ES00319.

Abbreviations used

ICP-MS	inductively coupled plasma mass spectroscopy
CDK	cyclin dependent kinase
YPD	yeast extract, peptone, dextrose medium
SC	synthetic complete medium
AAS	atomic absorption spectroscopy
O.D	optical density
SD	standard deviation

NIH-PA Author Manuscript

NIH-PA Author Manuscript

NIH-PA Author Manuscript

References

1. Frey CM, Banyasz JL, Stuehr JE. J Am Chem Soc 1972;94:9198–9204. [PubMed: 4345161]
2. Biaglow JE, Kachur AV. Radiat Res 1997;148:181–187. [PubMed: 9254738]
3. Barnese K, Gralla EB, Cabelli DE, Valentine JS. J Am Chem Soc 2008;130:4604–4606. [PubMed: 18341341]
4. Kumble KD, Kornberg A. J Biol Chem 1995;270:5818–5822. [PubMed: 7890711]
5. Lichko L, Kulakovskaya T, Pestov N, Kulaev I. Biosci Rep 2006;26:45–54. [PubMed: 16779667]
6. Keasling JD. Ann N Y Acad Sci 1997;829:242–249. [PubMed: 9472324]
7. Nagata T, Kiyono M, Pan-Hou H. Appl Microbiol Biotechnol 2006;72:777–782. [PubMed: 16514513]
8. Pan-Hou H, Kiyono M, Omura H, Omura T, Endo G. FEMS Microbiol Lett 2002;207:159–164. [PubMed: 11958934]
9. Martinez P, Persson BL. Mol Gen Genet 1998;258:628–638. [PubMed: 9671031]
10. Fristedt U, Weinander R, Martinsson HS, Persson BL. FEBS Lett 1999;458:1–5. [PubMed: 10518922]
11. Jensen LT, Ajua-Alemanji M, Culotta VC. J Biol Chem 2003;278:42036–42040. [PubMed: 12923174]
12. Lee YS, Huang K, Quiocho FA, O'Shea EK. Nat Chem Biol 2008;4:25–32. [PubMed: 18059263]
13. Wykoff DD, Rizvi AH, Raser JM, Margolin B, O'Shea EK. Mol Cell 2007;27:1005–1013. [PubMed: 17889672]
14. Kaffman A, Herskowitz I, Tjian R, O'Shea EK. Science 1994;263:1153–1156. [PubMed: 8108735]
15. Ogawa N, DeRisi J, Brown PO. Mol Biol Cell 2000;11:4309–4321. [PubMed: 11102525]
16. Wippo CJ, Krstulovic BS, Ertel F, Musladin S, Blaschke D, Sturzl S, Yuan GC, Horz W, Korber P, Barbaric S. Mol Cell Biol 2009;29:2960–2981. [PubMed: 19307305]
17. Serrano R, Ruiz A, Bernal D, Chambers JR, Arino J. Mol Microbiol 2002;46:1319–1333. [PubMed: 12453218]
18. Reddi AR, Jensen LT, Naranuntarat A, Rosenfeld L, Leung E, Shah R, Culotta VC. Free Radic Biol Med 2009;46:154–162. [PubMed: 18973803]
19. Portnoy ME, Jensen LT, Culotta VC. Biochem J 2002;362:119–124. [PubMed: 11829747]
20. Yang M, Jensen LT, Gardner AJ, Culotta VC. Biochem J 2005;386:479–487. [PubMed: 15498024]
21. Jensen LT, Culotta VC. J Mol Biol 2002;318:251–260. [PubMed: 12051835]
22. Rutherford JC, Ojeda L, Balk J, Muhlenhoff U, Lill R, Winge DR. J Biol Chem 2005;280:10135–10140. [PubMed: 15649888]
23. Yamaguchi-Iwai Y, Stearman R, Dancis A, Klausner RD. Embo J 1996;15:3377–3384. [PubMed: 8670839]
24. Sherman, F. Methods in Enzymology. Gurthie, C.; Fink, GR., editors. Academic Press; Orlando, FL: 1991.
25. Schmitt ME, Brown TA, Trumpower BL. Nucleic Acids Res 1990;18:3091–3092. [PubMed: 2190191]
26. Eide DJ, Clark S, Nair TM, Gehl M, Gribskov M, Guerinot ML, Harper JF. Genome Biol 2005;6:R77. [PubMed: 16168084]
27. Philpott CC, Protchenko O, Kim YW, Boretsky Y, Shakoury-Elizeh M. Biochem Soc Trans 2002;30:698–702. [PubMed: 12196168]
28. Yun CW, Bauler M, Moore RE, Klebba PE, Philpott CC. J Biol Chem 2001;276:10218–10223. [PubMed: 11120744]
29. Blaiseau PL, Lesuisse E, Camadro JM. J Biol Chem 2001;276:34221–34226. [PubMed: 11448968]
30. Rutherford JC, Jaron S, Winge DR. J Biol Chem 2003;278:27636–27643. [PubMed: 12756250]
31. Yamaguchi-Iwai Y, Dancis A, Klausner RD. Embo J 1995;14:1231–1239. [PubMed: 7720713]
32. Philpott CC, Protchenko O. Eukaryot Cell 2008;7:20–27. [PubMed: 17993568]
33. Waters BM, Eide DJ. J Biol Chem 2002;277:33749–33757. [PubMed: 12095998]

NIH-PA Author Manuscript

NIH-PA Author Manuscript

NIH-PA Author Manuscript

34. Wykoff DD, O'Shea EK. Genetics 2001;159:1491–1499. [PubMed: 11779791]
35. Sethuraman A, Rao NN, Kornberg A. Proc Natl Acad Sci U S A 2001;98:8542–8547. [PubMed: 11447286]
36. Hurlimann HC, Stadler-Waibel M, Werner TP, Freimoser FM. Mol Biol Cell 2007;18:4438–4445. [PubMed: 17804816]
37. Swinnen E, Rosseels J, Winderickx J. Curr Genet 2005;48:18–33. [PubMed: 15926040]
38. Wanke V, Pedruzzi I, Cameroni E, Dubouloz F, De Virgilio C. Embo J 2005;24:4271–4278. [PubMed: 16308562]
39. Dix DR, Bridgham JT, Broderius MA, Byersdorfer CA, Eide DJ. J Biol Chem 1994;269:26092–26099. [PubMed: 7929320]
40. Portnoy ME, Liu XF, Culotta VC. Mol Cell Biol 2000;20:7893–7902. [PubMed: 11027260]
41. Archibald FS, Fridovich I. Arch Biochem Biophys 1982;214:452–463. [PubMed: 6284026]

NIH-PA Author Manuscript
NIH-PA Author Manuscript
NIH-PA Author Manuscript

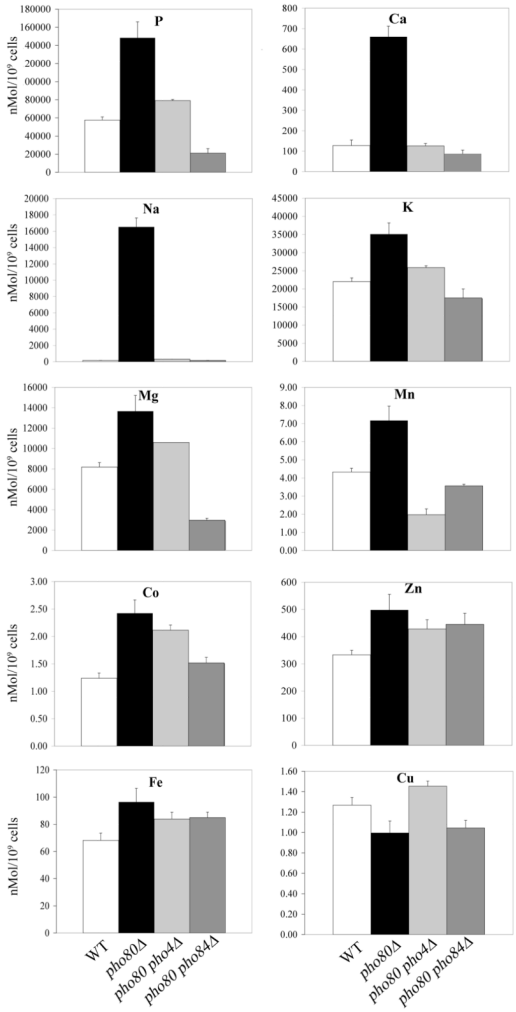

Figure 1. ICP-MS analysis of *pho80* mutants

Whole cell nitric acid digests of wild type cells (white bars, strain BY4741), *pho80*Δ (black bars, LR801), *pho80*Δ *pho4*Δ cells (grey bars, LR191) and *pho80*Δ *pho84*Δ (hatched bars, LR154) grown in enriched YPD medium were analyzed using ICP-MS. Results for the indicated elements are shown as averages from three independent cultures; error bars indicate standard deviation (S.D.).

NIH-PA Author Manuscript

NIH-PA Author Manuscript

NIH-PA Author Manuscript

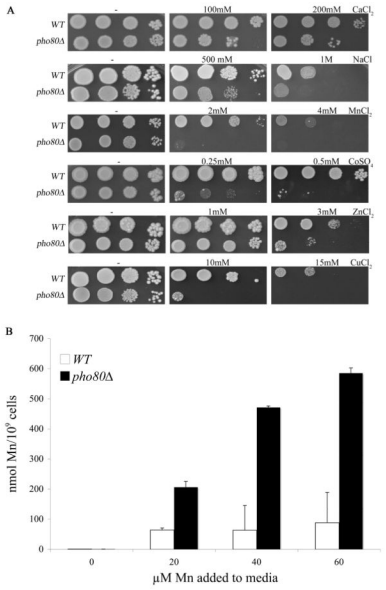

Figure 2. Effects of *pho80* mutations on metal toxicity and manganese accumulation

(A) Serial dilutions of WT and *pho80*Δ yeast were tested for growth on enriched YPD medium supplemented with the designated concentrations of metal salts as described in *Materials and Methods*.

(B) The WT and *pho80*Δ yeast were grown for 18 hours in enriched YPD medium supplemented with the indicated levels of $MnCl_2$ and whole cell levels of manganese were measured using AAS as described in *Materials and Methods*. Values are averages of duplicate measurements from two independent cultures, error bars indicate S.D. Strains are as described in Fig. 1.

NIH-PA Author Manuscript

NIH-PA Author Manuscript

NIH-PA Author Manuscript

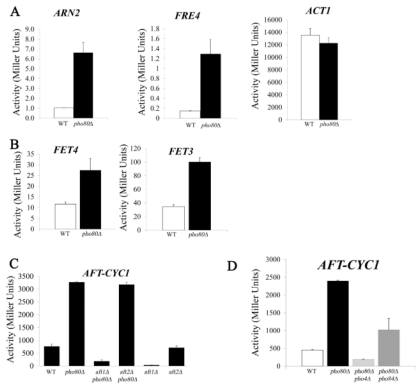

Figure 3. LacZ reporter assays for iron transport gene expression

The indicated yeast strains were transformed with the designated LacZ reporter plasmids. Duplicate cultures were grown in selecting minimal media (A, B left, C, D) or low phosphate minimal media (B right) for 16–18 hours and LacZ measurements conducted as described in *Materials and Methods*. Plasmids used contained the promoters for (A) *ACT1* (pLJ098), *ANR2* (pLJ439) and *FRE4* (pLJ441); (B) *FET3* (pLJ440) and *FET4* (pLJ051); (C-D) *AFT-CYC* representing the isolated Aft1p binding site from *FET3* fused to the core promoter for *CYC1* (pFC-W). Strains utilized: WT, BY4741; *pho80*, LR801; *aft1*Δ, LJ194; *aft1*Δ *pho80*Δ, LJ416; *aft2*Δ, 1090; *aft2*Δ *pho80*Δ, AR086; *pho80*Δ *pho4*Δ, LR191; and *pho80*Δ *pho84*Δ, LR154.

NIH-PA Author Manuscript
NIH-PA Author Manuscript
NIH-PA Author Manuscript

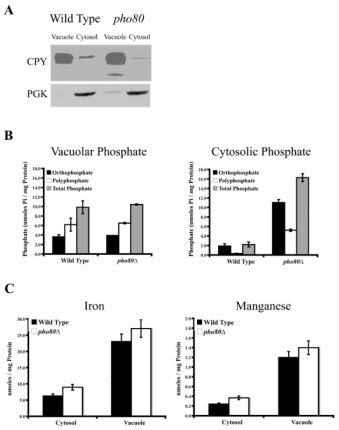

Figure 4. Vacuolar and cytosolic manganese, iron, and phosphate accumulation

(A) The purity of vacuolar and cytosolic fractional equivalents of wild type and *pho80*Δ strains were determined by immunoblot against CPY1 and PGK1, vacuolar and cytosolic biomarkers, respectively. Whole cell lysates were

(B) Total, ortho, and polyphosphate was measured using the colorimetric molybdate method described in the *Materials and Methods* for cytosolic and vacuolar fractions of the wild type and *pho80*Δ strains. The results are based on duplicate cultures, with the indicated error bars representing the standard deviation.

(C) Manganese and iron content of the cytosolic and vacuolar fractions of wild type and *pho80*Δ strains were measured by AAS. Measurements were done on duplicate samples, with the error shown as the standard deviation.

NIH-PA Author Manuscript
NIH-PA Author Manuscript
NIH-PA Author Manuscript

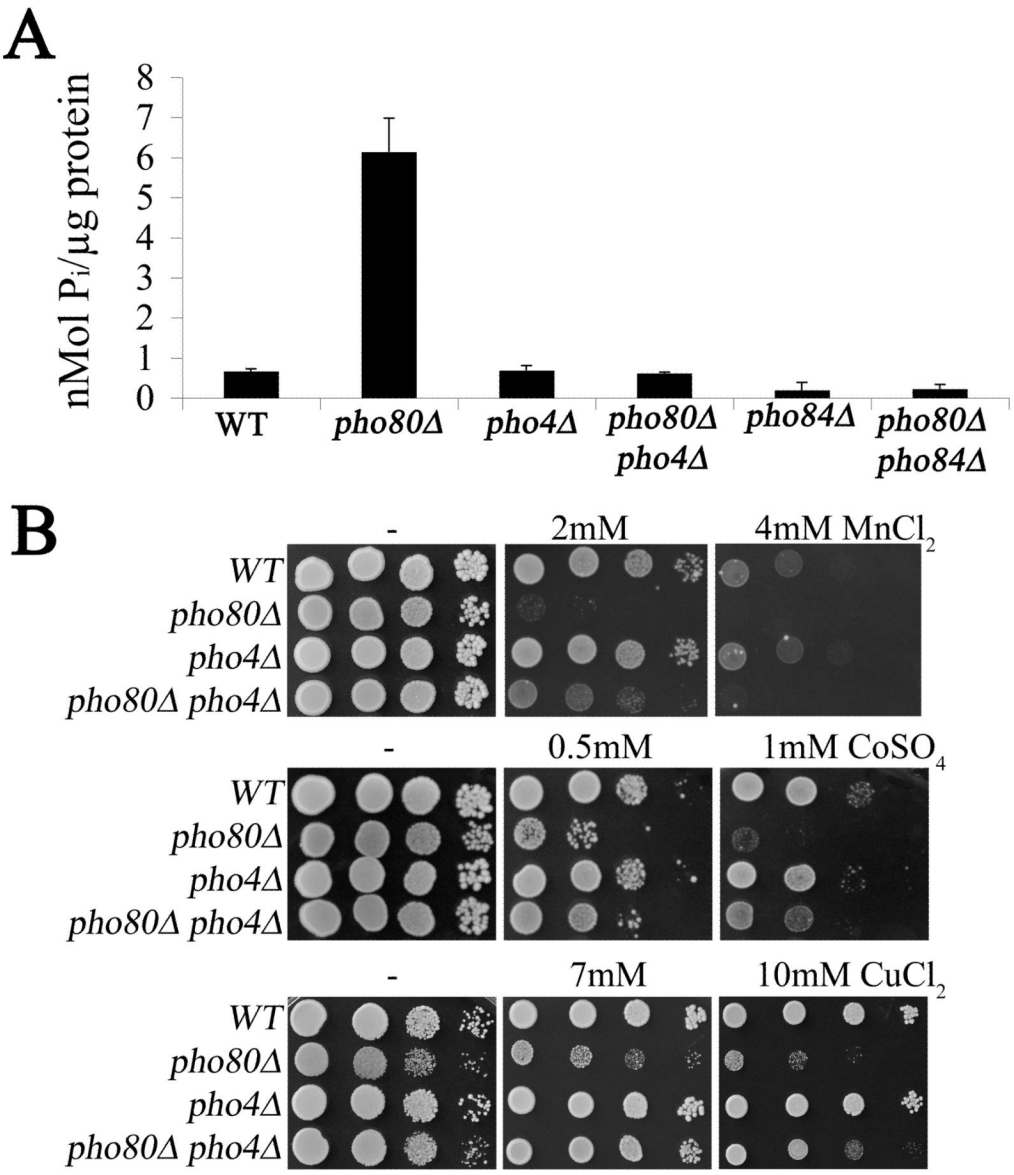

Figure 5. The effects of *pho4* mutation on *pho80* mutants

(A) Whole cell orthophosphate was assayed in the indicated strains using the molybdate method described in *Materials and Methods*. Results represent the averages of two independent cultures from independent experimental trials, error bar indicate S.D. (B) The indicated strains were tested for metal toxicity effects as in Fig. 2A. Strains utilized include: WT, BY4741; *pho80*Δ, LR801 panel A, LR237, panel B; *pho4*Δ, LR181; *pho80*Δ *pho4*Δ, LR191.

NIH-PA Author Manuscript

NIH-PA Author Manuscript

NIH-PA Author Manuscript

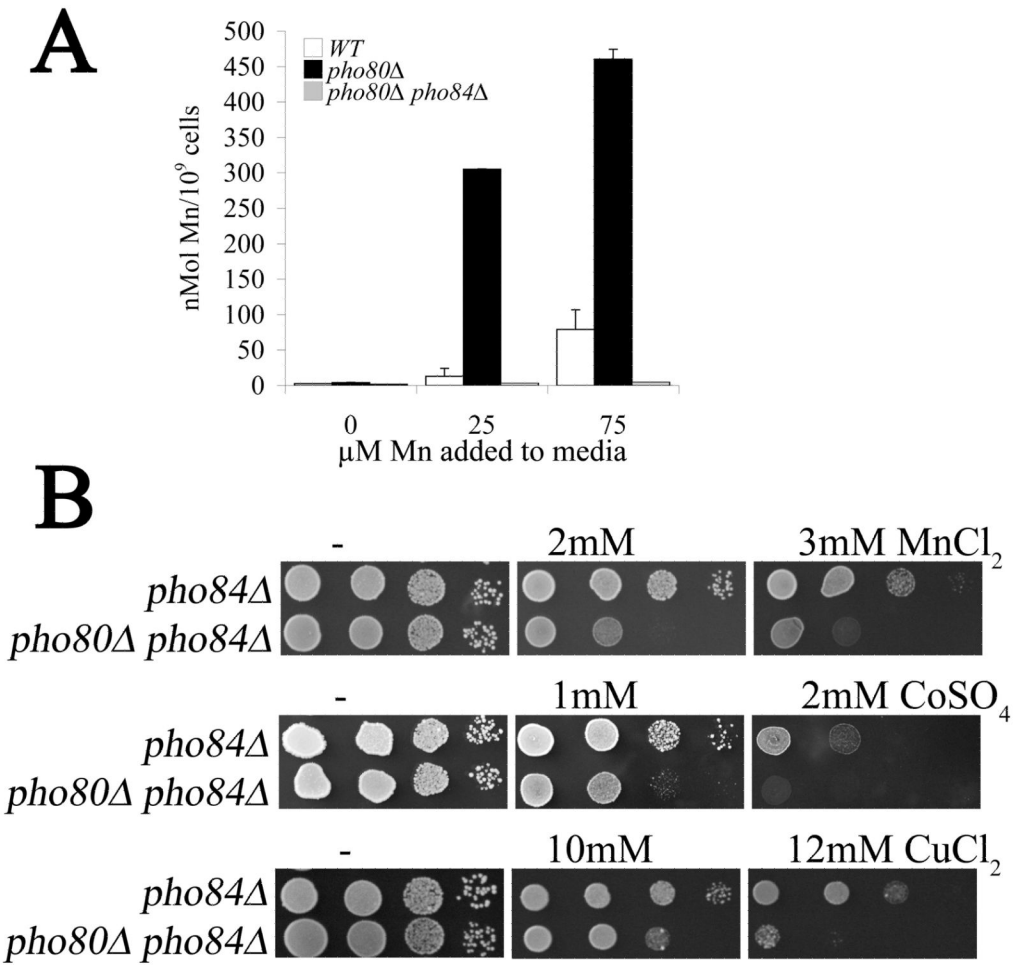

Figure 6. The Pho4p and Pho84p independent component to *pho80* metal toxicity

(A) Whole cell levels of manganese were measured using AAS in the indicated strains treated with the designated concentrations of manganese as described in Fig. 2B.

(B) Tests for metal toxicity were conducted as in Fig. 2A.

Strains utilized: *pho84*Δ, LR122; *pho80*Δ *pho84*Δ, LR154.

NIH-PA Author Manuscript

NIH-PA Author Manuscript

NIH-PA Author Manuscript

Table 1

Elemental concentrations by ICP-MS

Element	YPD (μM)	WT (μM)	*pho80*Δ (μM)
Na	16590 ± 58	2150± 250	236140 ± 15740
Mg	219.48 ± 1.29	116889 ± 6208	195190 ± 22010
P	13281 ± 49	823630 ± 51190	2118990 ± 252350
K	15307 ± 129	314430 ± 14620	501620 ±44160
Ca	67.78 ± 0.95	1817 ± 397	9428 ±742
Mn	0.708 ± .013	61.8 ± 2.9	102 ± 11.3
Fe	22.45 ± 0.25	973 ± 76	1377 ± 143
Co	1.015 ± 0.009	17.7 ± 1.3	34.6 ± 3.5
Cu	1.322 ± 0.018	18.12 ± 1.07	14.24 ± 1.66
Zn	61.53 ± 0.22	4760 ± 240	7117 ± 5.4

Samples were measured in three independent samples and value is show as ±S.D.

NIH-PA Author Manuscript

NIH-PA Author Manuscript

NIH-PA Author Manuscript

Table 2

Microarray detected changes in mRNA of phosphate metabolism and iron uptake genes

Standard Name	Systemic Name	Fold change*	Function
Phosphate regulated genes			
PHO5	YBR093C	4.72	acid phosphatase
PHO89	YBR296C	19.29	Na+/Pi cotransporter
PHM6	YDR281C	8.17	uknown function-regulated by phosphate
SPL2	YHR136C	2.93	similar to CDKI- phosphate regulated
Iron regulated genes			
ARN2	YHL047C	4.35	siderophore transporter
FIT2	YOR382W	3.48	siderophore retention
FIT3	YOR383C	2.58	siderophore retention
FRE4	YNR060W	11.79	ferric reductase for siderophore iron

* Fold change indicates the change in transcript between WT and *pho80*Δ cells

NIH-PA Author Manuscript

NIH-PA Author Manuscript

NIH-PA Author Manuscript

Table 3

Real time PCR analysis of transcripts in *pho80*Δ compared to WT cells

Gene	Fold Change*	lower bound**	upper bound***
PHO89	288.2	185.3	448.2
FRE4	54.1	45.7	64.1
PHM6	13.3	11.4	15.7
ARN2	10.7	9.6	12.0
PHO84	6.1	5.4	7.0

* Fold change is calculated as described in Experimental section, between the wild type strain and the isogeneic *pho80* mutant

** Lower bound (LB) was calculated using the standard deviation of three cultures such that LB=2^((ΔC$_T$(*pho80*)− ΔC$_T$(wild type))−standard deviation((ΔC$_T$(*pho80*)− ΔC$_T$(wild type)))

*** Upper bound (UB) was calculated using the standard deviation of three cultures such that UB=2^((ΔC$_T$(*pho80*)− ΔC$_T$(wild type))+standard deviation((ΔC$_T$(*pho80*)− ΔC$_T$(wild type)))